AIAA 2002–3158

Adaptive Identification and Control of Flow-Induced Cavity Oscillations

M. A. Kegerise
NASA Langley Research Center, Hampton, VA 23681

L. N. Cattafesta and C. Ha
University of Florida, Gainesville, FL 32611

1st AIAA Flow Control Conference
June 24–27, 2002/St. Louis, MO

Adaptive Identification and Control of Flow-Induced Cavity Oscillations

M. A. Kegerise*
NASA Langley Research Center, Hampton, VA 23681
L. N. Cattafesta† and C. Ha‡
University of Florida, Gainesville, FL 32611

Progress towards an adaptive self-tuning regulator (STR) for the cavity tone problem is discussed in this paper. Adaptive system identification algorithms were applied to an experimental cavity-flow tested as a prerequisite to control. In addition, a simple digital controller and a piezoelectric bimorph actuator were used to demonstrate multiple tone suppression. The control tests at Mach numbers of 0.275, 0.40, and 0.60 indicated ≈ 7dB tone reductions at multiple frequencies. Several different adaptive system identification algorithms were applied at a single freestream Mach number of 0.275. Adaptive finite-impulse response (FIR) filters of orders up to $N = 100$ were found to be unsuitable for modeling the cavity flow dynamics. Adaptive infinite-impulse response (IIR) filters of comparable order better captured the system dynamics. Two recursive algorithms, the least-mean square (LMS) and the recursive-least square (RLS), were utilized to update the adaptive filter coefficients. Given the sample-time requirements imposed by the cavity flow dynamics, the computational simplicity of the least mean squares (LMS) algorithm is advantageous for real-time control.

Introduction

THE flow over a cavity is characterized by a complex feedback process that leads to self-sustaining oscillations at a discrete set of frequencies. Often, these multiple "Rossiter modes" experience significant non-linear interactions and mode switching.[1,2] Cavity flows are of practical significance to aircraft with weapons bays. Here, the large sound pressure levels associated with the flow oscillations (> 170 dB) can be damaging to stores within the bay and can influence the trajectory of released stores. Cavity flows are also of interest as an active-control testbed. The problem is low-dimensional in the sense that only a few discrete modes are to be controlled, and only a small number of actuators and sensors are needed. This is in contrast to more complicated active control problems, such as turbulent boundary layer drag reduction, where the physics is infinitely dimensional and large numbers of distributed sensors and actuators are necessary.

Previous studies have considered the active control of cavity oscillations. Williams et al.,[2,3] employed a simple analog feedback controller to demonstrate multiple tone suppression at subsonic Mach numbers. Controller parameters were tuned manually to optimize suppression. While manual tuning of control parameters is not of practical interest, the experiments demonstrated the potential for feedback control. The controller also provides for quick evaluation of different actuator concepts. Cabell et al.[4] used discrete-time, linear quadratic control design methods for feedback control of cavity tones. The controller was successful in reducing the levels of multiple cavity tones at Mach numbers ranging from 0.275 to 0.45. Control performance was limited by excitation of sidebands of cavity tones, and the creation of new tones in the spectrum. These phenomena have recently been analyzed by Rowley et al.[5] and can, in part, be attributed to convective time delays between the actuator input and the output sensors (typically cavity-wall pressures). A linear quadratic regulator was also used by Cattafesta et al.[6] for single mode resonance at low Mach numbers (< 0.15).

An important limitation of standard feedback control schemes is that they cannot compensate for changes in system dynamics. The system dynamics of cavity flows change as flow conditions are altered. There is also the question of whether system dynamics change under the application of control. Either case necessitates re-identification of the system dynamics for control design. Adaptive controllers offer promise to overcome the limitations imposed by standard methods. They can adapt to changing flow conditions, can provide automatic tuning of controller parameters for optimal performance, and have built in system monitoring and fault tolerance. Adaptive controllers have already been applied to the cavity problem. Williams et al.[7] employed an adaptive feed-

*Research Scientist. Flow Physics and Control Branch. Member AIAA.

†Assistant Professor. Senior Member AIAA.

‡Graduate Research Assistant. Student Member AIAA

forward algorithm and achieved a 15 dB reduction in a single tone. However, the controller was unable to suppress multiple cavity tones. Cattafesta et al.[8] applied an adaptive disturbance rejection algorithm that uses an embedded ARMARKOV system identification model. Single-mode suppression of 10 dB was achieved, but limitations in the actuator prevented control of multiple modes.

The present work is focused on the development of a fully adaptive feedback controller that can maintain minimum sound pressure levels (SPL) over a range of subsonic Mach numbers. The adaptive controller of interest is the self-tuning regulator (STR) shown in Figure 1. The basic idea of the STR is to form an adaptive prediction of the system output and then determine the input by setting the predicted output equal to the desired value.[9] In cavity control, the problem is one of disturbance rejection. Therefore, the STR seeks to produce a control signal, $u(t)$, that will drive the system output, $y(t)$, to the desired value of zero. In the present case, an unsteady pressure signal from within the cavity represents the system output. The structure of the STR is quite general, and any appropriate model can be used to represent the system input-output dynamics (e.g., linear FIR and IIR filters). The parameters of the model, $\theta(t)$, are updated in real-time with a recursive parameter estimator and these in turn are used to form a one-step ahead predictor. To form the control law, the predicted output is set to zero and the resulting equation is solved for the required control signal.

This paper reports on our progress towards the application of an STR to the cavity control problem. As a first step to this end, a suitable actuator for cavity control was developed and characterized. This actuator was then used in a simple feedback controller to demonstrate multiple-mode suppression. Lastly, adaptive system identification algorithms were applied to the cavity flow to determine appropriate input-output models for control. A primary issue here is to determine the minimum model order that can capture the system dynamics within the computational constraints imposed by the real-time hardware.

The paper is organized as follows. The experimental details on the wind-tunnel, cavity model, actuator, and data systems are summarized. Next the baseline acoustic response of the cavity is presented, followed by the actuator transfer function measurements. Results from digital feedback control experiments with the actuator are then presented. Finally, the results of the system identification experiments are presented and discussed.

Experimental Details

Wind Tunnel Facility

The experimental program was conducted in the NASA-Langley Probe Calibration Tunnel (PCT). The

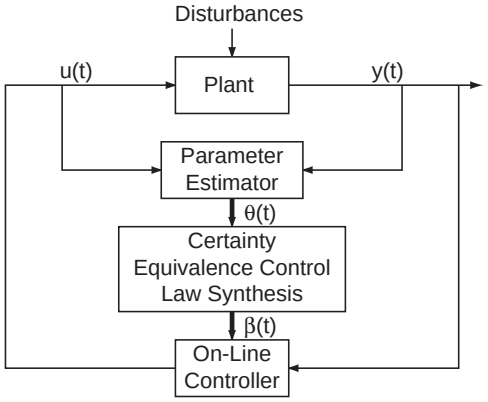

Fig. 1 Self-tuning regulator (STR).

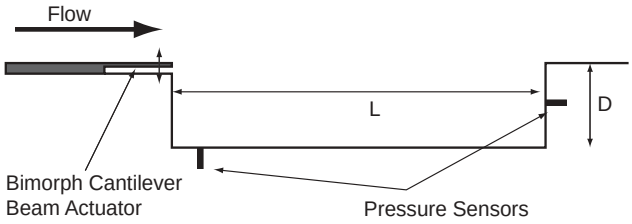

Fig. 2 Schematic of cavity model.

PCT is typically operated as an open-jet pressure tunnel with independent control of stagnation pressure, stagnation temperature, and free stream velocity. The stagnation pressure and temperature ranges for the facility are 13.8 kPa to 1034 kPa and 255 K to 367 K, respectively. For the current experiments, the facility was fitted with a subsonic nozzle that contracts from a circular inlet to a 50.8 mm by 152.4 mm exit. A straight duct section of length 0.6 m was attached to the nozzle exit and was terminated with a small-angle diffuser. The free stream Mach number range for the present tunnel configuration was 0.04 to 0.8.

Cavity Model

A rectangular cavity model was installed in the ceiling of the straight duct section of the PCT. The floor of the duct section was a foam filled baffle that minimized reflections of acoustic waves radiated by the cavity. The cavity model had a fixed length, $\ell = 152.4$ mm, and a variable depth, d, which was fixed to 30.48 mm, for an ℓ/d ratio of 5. The cavity model spanned the width of the test section ($w = 50.89$ mm) to provide an un-obscured view of the cavity shear layer for optical diagnostics.

The cavity model was instrumented with a pair of piezoresistive pressure transducers. The sensors has a nominal sensitivity and bandwidth of 2.2×10^{-5} V/Pa and 14 kHz, respectively. One sensor was located in the floor midplane, 18 mm downstream from the cavity front wall. The second sensor was located in the midplane of the rear cavity wall, 19 mm from the cavity trailing edge. A schematic of the cavity is shown in Figure 2, with actuator and sensor locations indicated.

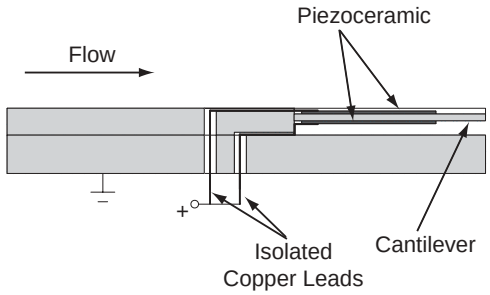

Fig. 3 Schematic of piezoelectric bimorph actuator assembly.

Piezoelectric Bimorph Actuator

In cavity control, the objective of the actuator is to produce a disturbance equal and opposite to the natural one produced by acoustic feedback. To meet this objective, any actuator for cavity control must meet a certain set of requirements. The actuator must have a bandwidth as large as the maximum Rossiter frequency of interest (~ 1 kHz in the present case). The requirements for the actuator amplitude response are not known a priori because the disturbance levels at the shear-layer origin are not typically known. However, it is desired to have a response that can produce a broadband disturbance rather than a single tone. Finally, the actuator should be situated such that it introduces disturbances at the cavity leading edge where the flow is most receptive. A flap-type actuator provides a good balance between these requirements and was thus chosen for the present work.

The flap-type actuator is a piezoelectric bimorph cantilever beam. Figure 2 shows the actuator installation in the wind-tunnel model. The tip of the beam is coincident with the cavity leading edge. The actuator was designed with a structural dynamics model and an optimization scheme. Given a desired natural frequency, the design parameters are calculated such that the target frequency is achieved and tip displacement is maximized. The target frequency for the present actuator was 1500 Hz and the calculated DC gain was $0.25\ \mu m/V$. Further details of the design methodology are beyond the scope of this work and the interested reader can refer to the papers by Cattafesta et al.[10,11]

Table 1 Design parameters of piezoelectric bimorph actuator.

Quantity	Value
Shim length, mm	25.4
Piezo length, mm	17.8
Shim thickness, mm	0.89
Piezo thickness, mm	0.38
Shim width, mm	48.0
Piezo width, mm	48.0

A schematic of the bimorph actuator assembly is shown in Figure 3 and a listing of the design parameters is provided in Table 1. The cantilever beam portion of the actuator was machined from aluminum. The piezoceramic wafers (PZT 5H) were bonded to the cantilever beam with a non-conductive epoxy adhesive. The actuator structure and cantilever beam were electrically grounded for safety reasons. High voltage was applied to the electrodes of the piezoceramics with isolated copper flat leads in a parallel configuration. A fairing layer of Kapton was placed on the top surface of the cantilever structure to provide a smooth surface for the incoming boundary layer.

A fiber-optic sensor was embedded in the front wall of the cavity model to provide an in situ measurement of the actuator displacement. Due to physical constraints imposed by the cavity model design, it was not possible to place the sensor at the actuator tip. Instead, the actuator was located 4 mm from the tip and offset 9 mm from the actuator centerline.

The in situ measurement of displacement is important for several reasons. The actuator frequency response can be measured in wind-on and wind-off conditions. This measurement will answer the question of whether flow over the actuator surface changes the dynamic response. More importantly, the displacement levels necessary for suppression of cavity tones can be quantified. This information can then be fed back into the design stage for future actuator generations.

Data Acquisition and Processing

The data acquisition and processing systems are described in this section. Depending on the purpose of the experiments, three different data systems were used.

To measure the bimorph transfer function, the actuator was excited with a chirp signal produced by a function generator. The frequency of the chirp signal was swept from 10 Hz to 2 kHz in 200 msec. The chirp signal was input to a high-voltage amplifier with a nominal gain of 100. The output of the amplifier was applied to the bimorph actuator. The signals from the function generator (input) and the displacement sensor (output) were bandpass filtered from 1 Hz to 4 kHz and sampled at 10.24 kHz with a 16-bit A/D. The data were subsequently processed to produce estimates of the transfer function.

For the digital control experiments, the front-wall pressure (error signal) was amplified to ± 10 V and bandpass filtered from 1 Hz to 16 kHz. This signal was sampled at 40 kHz with a 16-bit A/D card of a dSPACE digital control system. The real-time controller calculated the control signal once per time step using a single-processor dSPACE DS1005 card that utilizes a PowerPC7509 processor running at 480 MHz. The digital control signal was converted to the analog domain with a 14-bit D/A card. The control signal was routed to a reconstruction filter ($f_{cut} = 16$ kHz) to smooth the zero-order hold signal from the D/A card.

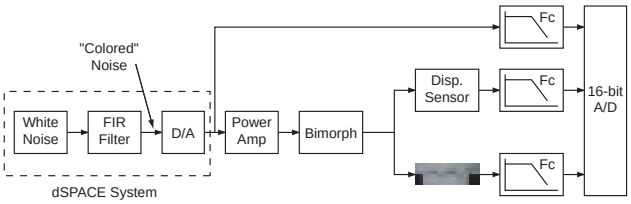

Fig. 4 Schematic of data acquisition system for system identification experiments.

The resulting signal was input to the high-voltage amplifier before passing into the bimorph actuator.

A schematic of the data acquisition system for the system identification experiments is shown in Figure 4. The dSPACE real-time processor was used to generate bandlimited colored noise. The spectral shape of the noise signal was such that the actuator tip displacement was bandlimited white noise. In effect, the FIR filter noted in Figure 4 is the inverse transfer function of the bimorph actuator. The noise was input to the high-voltage amplifier before passing into the actuator. The amplifier input voltage, the displacement sensor signal, and the wall pressure signals were each amplified and then bandpass filtered from 1 Hz to 2.2 kHz. The signals were sampled at 5.12 kHz by the 16-bit A/D card on the dSPACE system. Several adaptive system identification algorithms were coded in SIMULINK and converted to compiled code to be run on the dSPACE DS1005 card. The algorithms were used to identify the transfer function between the input samples (amplifier input voltage or actuator displacement) and the output samples (wall pressure sensors).

Test Conditions

All measurements presented were performed on a cavity with length-to-depth ratio of 5. Cavity control experiments and actuator transfer function measurements were performed at three conditions: 1) $M_\infty = 0.275$, $Re/m = 8.1\times10^6\ m^{-1}$, 2) $M_\infty = 0.40$, $Re/m = 11.4\times10^6\ m^{-1}$, and 3) $M_\infty = 0.60$, $Re/m = 8.0\times10^6\ m^{-1}$. The system identification experiments presented in this paper were performed at a single Mach number of 0.275 and $Re/m = 8.1\times10^6\ m^{-1}$.

Results and Discussion

Baseline Flow

The acoustic response of the $\ell/d = 5$ cavity was determined using the pressure sensors located in the front floor and rear wall of the model. The coherence between these two sensors was used to identify those peaks in the autospectrum that correspond to Rossiter modes. The amplitude and frequency of the peaks were extracted from the rear-wall pressure autospectrum, and the Strouhal number ($St_\infty = f\ell/U_\infty$) of the oscillations was calculated. These were compared to the modified Rossiter equation:[12]

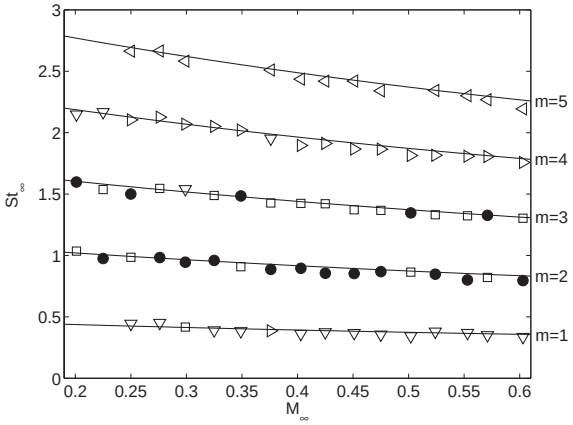

Fig. 5 Acoustic response of $\ell/d = 5$ cavity.

$$St_\infty = \frac{m-\alpha}{M_\infty\left(1+\frac{\gamma-1}{2}M_\infty^2\right)^{-1/2}+1/k}, \qquad (1)$$

where m is the (integer) mode number, and $\alpha = 0.25$ and $k = 0.66$ are empirical constants. The results are presented in Figure 5, where the symbols denote experimental data and the lines are calculated from the Rossiter equation. As seen in the figure, the agreement is very good, verifying that the present model behaves as expected.

Actuator Transfer Function Measurements

The results of the actuator transfer function measurements are shown in Figure 6. Measurements were made for three flow conditions and the wind-off condition. The data indicate that flow has no significant influence on the actuator dynamic response over the range of flow conditions tested. This allays previous concerns that fluid loading damps the response of the actuator and limits the performance of an active controller.[8] Furthermore, the transfer function was found to be repeatable over several months of testing.

The natural frequency of the present actuator is seen to be ≈ 1200 Hz, while the DC gain is $\approx 0.25\ \mu m/V$. The measured DC gain is in good agreement with the predicted value of the structural dynamics model. The natural frequency falls short of the designed value of 1500 Hz. This may be due, in part, to compliance at the cantilever root line. Measurements of the displacement at the root line were found to be nonzero. The design model, however, assumes a perfect clamp. Nevertheless, the actuator bandwidth is suitable for control of several Rossiter modes over the Mach number range tested.

Digital Feedback Control Experiments

In this section, feedback control experiments with a simple digital controller are presented. The primary objectives of these control experiments were: 1) determine the suitability of the actuator for suppression of multiple cavity modes and 2) quantify the displacement levels necessary for suppression.

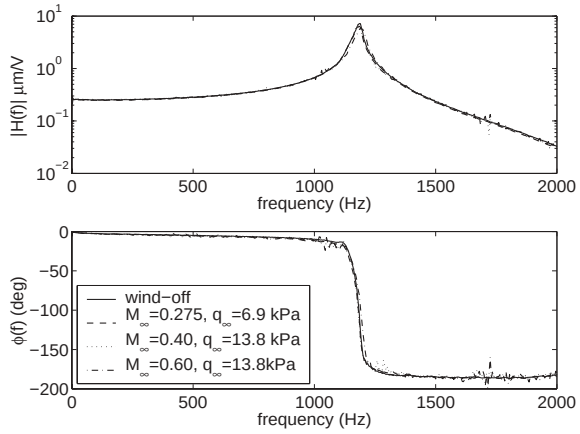

Fig. 6 Frequency response function of the piezoelectric bimorph actuator

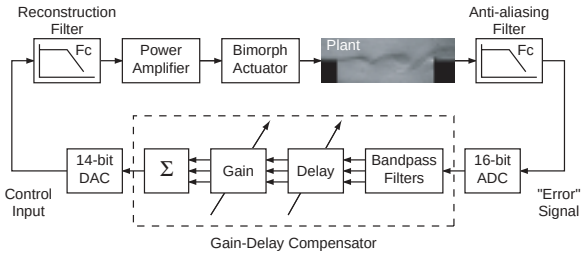

Fig. 7 Digital gain-delay feedback controller.

A schematic of the feedback controller is shown in Figure 7. The primary component of the controller consists of a gain-delay compensator that was programmed in SIMULINK and converted to compiled code that runs on the dSPACE DS1005 card. The sample time for the controller was 25 μsec. The compensator processes the "error" signal (front-floor pressure) as follows. The error signal is passed through a bank of digital bandpass filters (4th-order elliptic filters). Each filter is centered on a particular Rossiter mode. The signals from the digital filters are then passed through a delay of n samples and a gain a K. Note that these values are different for each Rossiter mode. Finally, the resulting signals are summed and output from the dSPACE system via the 14-bit D/A card. The parameters of the gain and delay blocks are tuned manually to minimize some performance measure. In the present case, the rear-wall pressure sensor was considered to be the performance measure and the compensator parameters were adjusted to minimize the tonal levels of each Rossiter mode lying within the actuator bandwidth. It should be noted that this type of controller is not new. Recently, Williams et al.[2,3] utilized this controller (in both the analog and digital domain) for cavity control studies. The gain-delay compensator was also used for feedback control of impinging-jet resonance[13] and vortex shedding from a cylinder in cross flow.[14]

Typical control results for three test conditions are shown in Figures 8, 9, and 10. The plots present

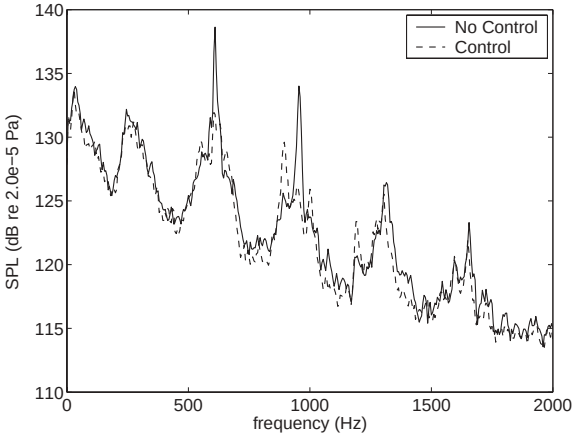

Fig. 8 Control performance at M_∞ = 0.275.

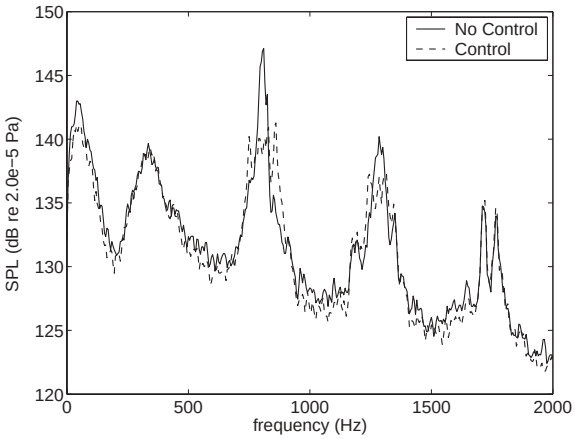

Fig. 9 Control performance at M_∞ = 0.40.

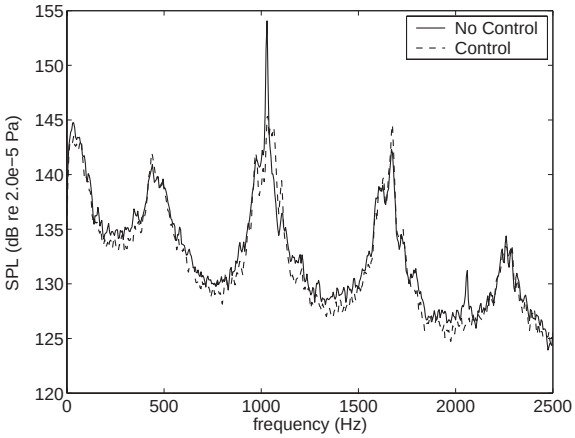

Fig. 10 Control performance at M_∞ = 0.60.

the rear-wall autospectrum with and without control. Similar results were found for the front-floor pressure spectrum. As seen in the figures, the dominant Rossiter mode is typically suppressed by more the 7 dB for the three cases tested. In addition, it is observed that the bimorph actuator is capable of suppressing multiple cavity modes (see Figures 8 and 9). In the $M_\infty = 0.60$ case, only the dominant Rossiter mode ($m = 2$) is suppressed since the higher modes lie outside the actuator bandwidth. Also in this case, the first harmonic of the dominant Rossiter mode (~ 2100 Hz) is present in the no-control autospectrum. With control, the harmonic is considerably reduced.

In many of the cases considered, the performance of the controller was limited by the excitation of sideband modes about a Rossiter mode. Rowley et al.[5] used a physics-based model of the cavity flow and the gain-delay controller to analyze the problem. From that analysis, it was concluded that delays in the plant (arising from the finite convection time between an input at the cavity leading edge and the output at the pressure sensor locations) and delays produced by the bandpass filters were responsible.

It is of interest to consider the displacement levels that are necessary for suppression of cavity tones as this knowledge will aid in future flap-actuator designs. The RMS tip displacement under control was found to range from 12 μm at $M_\infty = 0.275$ to 34 μm at $M_\infty = 0.60$. To place these deflection magnitudes in perspective, consider the incoming turbulent boundary in the present work. The boundary layer thickness is approximately 5 to 6 mm and one wall unit is approximately 2 μm. The required displacement levels under control thus lie in a region of the boundary layer ranging from $y^+ = 6$ to 17 wall units. These deflection levels are remarkably small, being on the order of the viscous sublayer. This bodes well for the use of flap-type actuators in cavity control. While tip displacements for frequencies away from resonance are only on the order of tens of micrometers, the present results suggest that this is sufficient for control. Driving flap-type actuators at frequencies away from resonance may also provide stability in their long term performance characteristics.

Recently, Cattafesta et al.[10] developed a fluid-structure coupling model to explain why flap actuators are effective. That analysis linked the streamwise perturbations produced by the flap actuator to mean velocity gradients in the near-wall region of the boundary-layer. For a turbulent boundary layer, these gradients are large and $u'/U_\infty \sim 0.25$ can be easily achieved with modest tip deflections.

Adaptive System Identification Experiments

A prerequisite for application of the self-tuning regulator is adaptive system identification. System identification involves the determination of a mathematical model from experimental input-output data.[15] In the present case, the input signal is the actuator input and the output signal is from one of the wall pressure sensors. A block diagram of the process is shown in Figure 11. An excitation signal (bandlimited white noise or a chirp signal) is input to both the unknown system and the adaptive filter. The desired output, $d(t)$, is compared to the adaptive filter output, $y(t)$, and a recursive algorithm is used to minimize the mean-squared error between them.

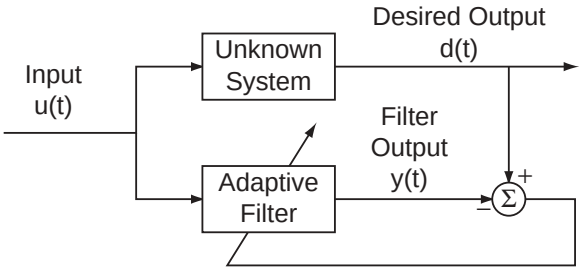

Fig. 11 System identification of a SISO system using an adaptive filter.

Two model structures were used in the present study: linear FIR and IIR filters. The output of an FIR filter is a moving average of the input. An FIR filter of length N is expressed as:

$$y(n) = \sum_{i=0}^{N-1} b_i(n) u(n-i), \tag{2}$$

where y is the output, u is the input, n is discrete sample time, and $b_i(n)$ are the filter coefficients. An advantage of FIR filters is that they are inherently stable due to their all-zero structure. The output of IIR filters is the weighted sum of previous inputs and outputs. An IIR filter of length N is expressed as:

$$y(n) = \sum_{i=1}^{N-1} a_i y(n-i) + \sum_{i=0}^{M-1} b_i u(n-i). \tag{3}$$

IIR filters are characterized by both poles and zeros, and therefore, stability is not guaranteed.

The model coefficients are updated at each time step by a recursive algorithm. Two well-known recursive algorithms were utilized: the least-mean squares (LMS) and the recursive least squares (RLS). The LMS algorithm is simple to implement and is the computationally least expensive adaptive algorithm. The operations per time step for the LMS algorithm are $\mathcal{O}(N)$. The RLS algorithm has a faster convergence rate toward the minimum mean-square error, but is computationally more expensive. The operations per time step for this algorithm are $\mathcal{O}(N^2)$. For IIR, the recursive algorithms can be broken down further into equation-error (EE) and output-error (OE) formulations. See Shynk[16] for details on these formulations. The reader can refer to any standard text on adaptive filtering for the general details of these algorithms.[17]

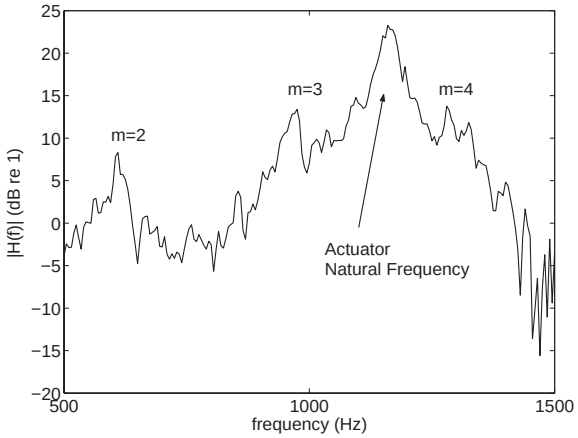

Fig. 12 Measured transfer function magnitude between actuator input and rear-wall pressure.

An important issue in adaptive control is that all computations must be completed within the sampling interval. The sampling interval is dictated by the frequency content of the process to be controlled. According to the Nyquist criterion, the sampling rate must be at least twice the highest frequency of interest. In the present case of cavity flow control, a sampling frequency of 5.12 kHz is desirable (sampling time of 195.3 μsec). The turnaround time, T_a, is defined as the time required to perform all the necessary calculations for a particular algorithm. Obviously, this must be smaller than the sample time, T_s. Further, the turnaround time associated with system identification should be somewhat less that the sample time to allow for the computations needed by the adaptive control scheme.

The system identification algorithms were applied to a single flow condition ($M_\infty = 0.275$). This flow condition is attractive because there are three Rossiter modes within the actuator bandwidth and therefore offers the greatest challenge to the identification algorithms. The actuator was driven with bandlimited (500-1500 Hz) colored noise (as described earlier) and the wall-pressure sensor signals were acquired. Prior to running the algorithms, input-output time series were recorded and the transfer function between them was calculated. This calculation was performed with standard FFT-based methods applied to 1024 point blocks, a Hanning window with 50% overlap, and 160 block averages. The result will be compared to the transfer functions identified by the adaptive algorithm in the following discussion. The transfer function magnitude between the input and output (rear-wall pressure) is shown in Figure 12. The figure is annotated to show the peaks associated with Rossiter modes $m = 2, 3, 4$. The large gain in the vicinity of 1200 Hz is due to the actuator dynamics. The magnitude of the transfer function outside of the 500-1500 Hz band is meaningless since there is no input.

Adaptive FIR Filter Results

Results for the FIR-LMS algorithm are shown in Figures 13a and 13b. The filter order for the data shown is $N = 100$. The turnaround time of this algorithm and filter order was 64 μsec. Time series of the system output (rear-wall pressure) and the adaptive filter output are shown in Figure 13a. The error between them, $d(n) - y(n)$, is also shown. As seen in the figure, the error between these two signals is significant.

The coefficients of the adaptive filter vary somewhat over time, and so the "instantaneous" transfer function varies with time. However, the coefficients vary about well defined mean values, suggesting some level of time invariance in the process. It is of interest then to consider whether the coefficients of the filter represent a transfer function that is, in an average sense, the measured transfer function of the system. To this end, the transfer function obtained from the filter coefficients at each time step was block averaged (in total, 2048 averages were used). The results are shown in Figure 13b. As observed in the figure, this average transfer function is not a good representation of the system dynamics.

Results for the FIR-RLS algorithm are shown in Figure 13c and 13d. The maximum filter order in this case was limited to $N = 20$, with a turnaround time of 136 μsec. It is clear that the computational requirements for the RLS algorithm are higher than for the LMS algorithm. This lower-order filter does a poor job of identifying the system dynamics.

Adaptive IIR Filter Results

Results for the adaptive IIR filters are shown in Figure 14. Adaptive IIR-LMS equation-error results are shown in Figure 14a and 14b. Here, the order of the moving-average coefficients was $M = 60$ and the order of the auto-regressive coefficients was $N = 100$. This filter does a good job of identifying the system dynamics in both the time and frequency domains. As seen in Figure 14b, the transfer function of the adaptive filter matches the measured transfer function in the vicinity of the Rossiter modes. The dynamics in the vicinity of the actuator natural frequency are, however, poorly matched. It is of interest to note that the turnaround time for this algorithm was 85 μsec. Thus, relatively high-order filters can be used while leaving computational resources for controller calculations.

The results for the adaptive IIR-LMS output-error algorithm are not shown. This is because the adaptive filter was not stable for any combination of filter parameters. Recall that the stability of IIR filters is not guaranteed. Further study is required to better understand the failure of this algorithm.

The IIR-RLS equation-error results are shown in Figure 14c and 14d. The maximum filter order that could be run in real-time was of 14th-order. The

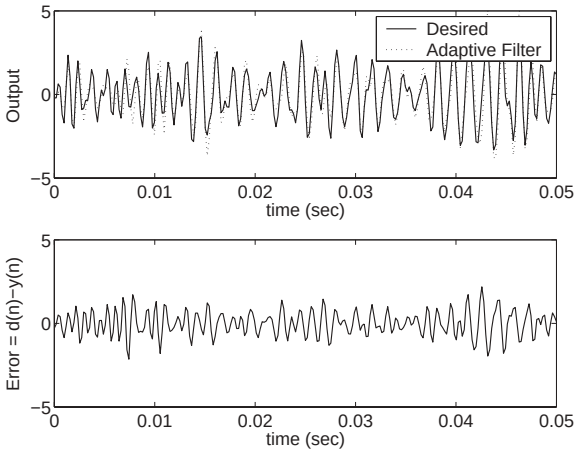

a) FIR LMS algorithm (N = 100).

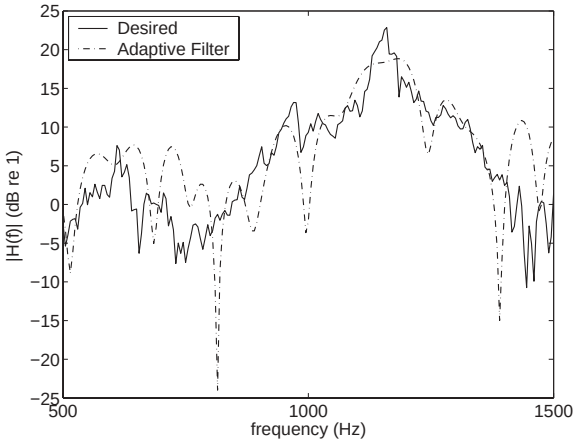

b) Measured and modeled transfer function magnitude from actuator to rear-wall pressure sensor (FIR LMS, N = 100).

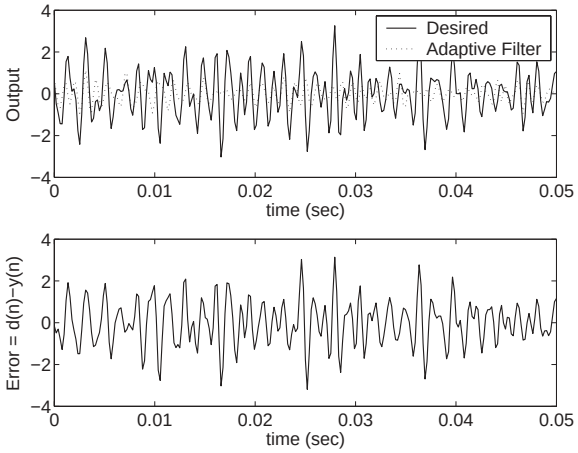

c) FIR RLS algorithm (N = 20).

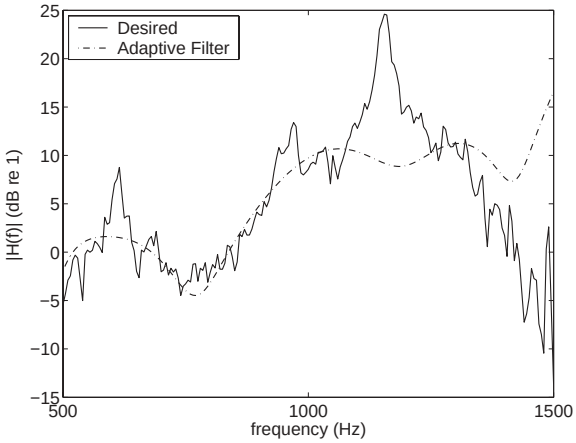

d) Measured and modeled transfer function magnitude from actuator to rear-wall pressure sensor (FIR RLS, N = 20).

Fig. 13 Comparison of adaptive FIR filters to measured response.

turnaround time was 141 μsec. This high value for turnaround time at low filter orders is indicative of the computational complexity of the RLS algorithm. In the time domain, the adaptive filter output matches the desired response quite well. In the frequency domain, the filter transfer function is a poor representation of the system dynamics, except near Rossiter modes 2 and 4. The inability of the adaptive filter to properly model the system dynamics is most likely due to the low order of the filter. The good agreement of the filter output in the time domain may be related to the fact that the largest portion of signal energy is in Rossiter mode 2. Here, the adaptive filter transfer function reasonably matches the measured value.

The filter order for the IIR-RLS output-error algorithm was similarly limited to 14th-order. The performance of this adaptive filter is poor in both the time and frequency domain (Figures 14e and 14f). The is particularly true in the frequency range around Rossiter mode 2. In the output-error formulation of adaptive IIR filters, the mean-square error system can have local minima.[16] Depending on the initial conditions for the filter, the adaptive algorithm may converge to one of these local minima rather than the global one. This may be responsible for the behavior observed in the present case.

In view of the present results the following general comments are made. It appears that adaptive filters that capture the system dynamics in the vicinity of the dominant Rossiter mode perform well in the time domain. IIR filters perform better than FIR filters of comparable order. Given that IIR filters have both pole and zeros, they are better suited for modeling of systems with resonances, as in the present case. The IIR-LMS algorithm is attractive because of its computational simplicity. Relatively large filter orders can be used while leaving some computational resources available for controller calculations.

Finally, the present results are not sufficient to answer the question of required model order. It is certain

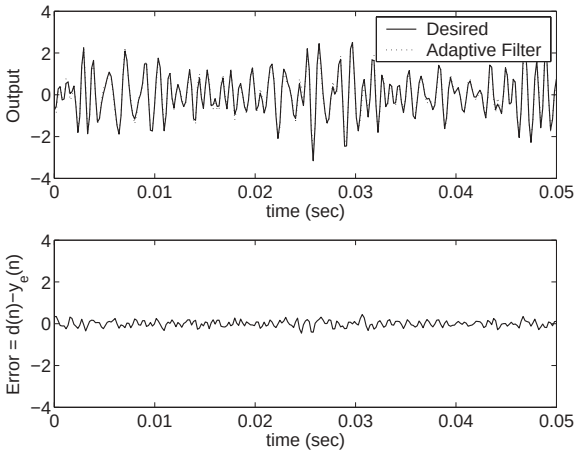

a) IIR LMS equation-error algorithm (M = 60, N = 100).

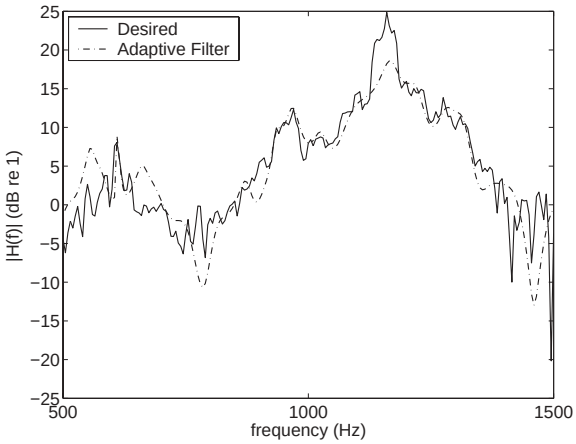

b) Measured and modeled transfer function magnitude from actuator to rear-wall pressure sensor (IIR LMS equation-error, M = 60, N = 100).

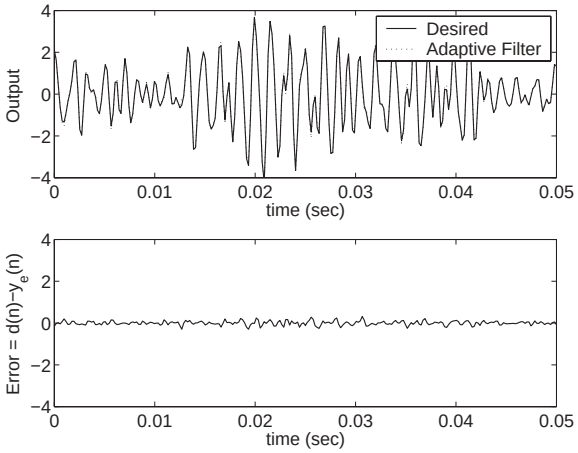

c) IIR RLS equation-error algorithm (M = 14, N = 14).

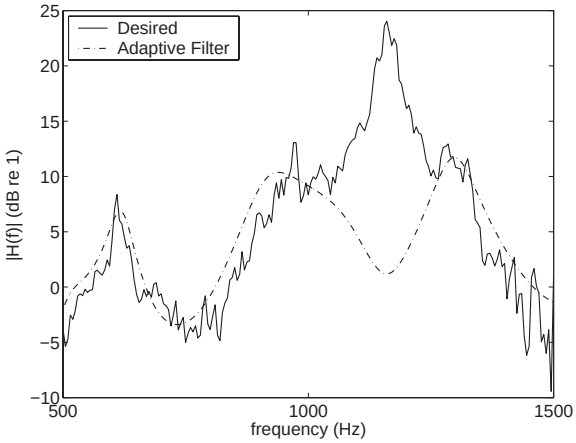

d) Measured and modeled transfer function magnitude from actuator to rear-wall pressure sensor (IIR RLS equation-error, M = 14, N = 14).

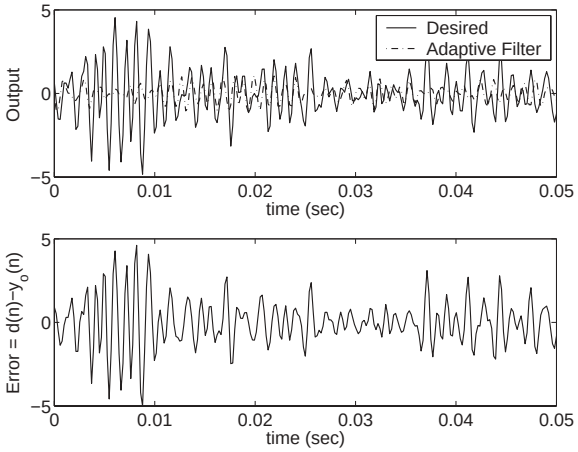

e) IIR RLS output-error algorithm (M = 14, N = 14).

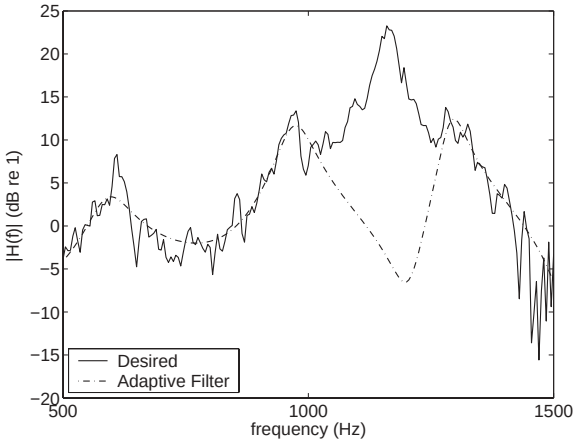

f) Measured and modeled transfer function magnitude from actuator to rear-wall pressure sensor (IIR RLS output-error, M = 14, N = 14).

Fig. 14 Comparison of adaptive IIR filters to measured response.

that the model order must be high enough to capture the system dynamics in the vicinity of the Rossiter modes. Since the objective of the control is tone reduction and not broadband noise reduction, the system dynamics between Rossiter modes may not have to be well modeled. Adaptive control tests with various filter orders are required to answer these questions.

Conclusions and Future Work

This paper reported on our progress towards an adaptive controller for cavity tone suppression. A particular control structure of interest is the self-tuning regulator (STR). To this end, a piezoelectric bimorph flap actuator was first developed and characterized. This actuator was chosen for its relatively high bandwidth (~ 1 kHz) and ability to generate large streamwise disturbances. The bimorph actuator was then used in a simple digital feedback controller to demonstrate its ability to control multiple cavity tones over a range of Mach numbers. The central feature of an STR is adaptive system identification. Therefore, several adaptive system identification algorithms were tested in this study to determine their suitability for modeling of the system dynamics.

Digital feedback control experiments were performed at three freestream Mach numbers ($M_\infty = 0.275, 0.40, 0.60$). The results demonstrate multiple tone suppression of up to 7 dB. An in situ measurement of the actuator tip displacement indicated that tip deflections on the order of the viscous sublayer of the incoming turbulent boundary layer were sufficient for control.

In the adaptive system identification experiments, two filter structures (FIR and IIR) and two recursive algorithms (LMS and RLS) were employed. Adaptive FIR filters of orders up to $N = 100$ were found to be unsuitable for modeling of the cavity flow dynamics. Adaptive IIR filters of comparable order were found to suitably represent the system dynamics. Because of their computational simplicity, adaptive IIR-LMS filters of much higher-order than IIR-RLS filters can be realized within the required sample times. The higher-order IIR-LMS filters were better able to capture the system dynamics and may be better suited to active control of cavity oscillations.

Future work will consider the use of the present algorithms at higher subsonic Mach numbers (up to $M_\infty = 0.6$). The system identification algorithms will then be used in the self-tuning regulator for control studies.

References

[1]Cattafesta, L. N., Garg, S., Kegerise, M. A., and Jones, G. S., "Experiments on Compressible Flow-Induced Cavity Oscillations," AIAA Paper 98–2912, June 1998.

[2]Williams, D. R., Fabris, D., Iwanski, K., and Morrow, J., "Closed-Loop Control in Cavities with Unsteady Bleed Forcing," AIAA Paper 2000–0470, Jan. 2000.

[3]Williams, D. R., Fabris, D., and Morrow, J., "Experiments on Controlling Mulitple Acoustic Modes in Cavities," AIAA Paper 2000–1903, June 2000.

[4]Cabell, R. H., Kegerise, M. A., Cox, D. E., and Gibbs, G. P., "Experimental Feedback Control of Flow Induced Cavity Tones," AIAA Paper 2002–2497, June 2002.

[5]Rowley, C. W., Williams, D. R., Colonius, T., Murray, R. M., MacMartin, D. G., and Fabris, D., "Model-Based Control of Cavity Oscillations Part II: System Identification and Analysis," AIAA Paper 2002–0972, Jan. 2002.

[6]Cattafesta, L. N., Garg, S., Choudhari, M., and Li, F., "Active Control of Flow-Induced Cavity Resonance," AIAA Paper 97–1804, June 1997.

[7]Williams, D. R. and Morrow, J., "Adaptive Control of Multiple Acoustic Modes in Cavities," AIAA Paper 2001–2769, June 2001.

[8]Cattafesta, L. N., Shukla, D., Garg, S., and Ross, J. A., "Development of an Adaptive Weapons-Bay Supression System," AIAA Paper 99–1901, June 1999.

[9]Goodwin, G. C. and Sin, K. S., Adpative Filtering Prediction and Control, Prentice-Hall, Englewood Cliffs, NJ, 1984.

[10]Cattafesta, L. N., Garg, S., and Shukla, D., "Development of Piezoelectric Actuators for Active Flow Control," AIAA Journal, Vol. 39, No. 8, Aug. 2001, pp. 1562–1568.

[11]Cattafesta, L. N., Mathew, J., and Kurdila, A., "Modeling and Design of Piezoelectric Actuators for Fluid Flow Control," AIAA Paper 2000-5534, Oct. 2000.

[12]Heller, H. H., Holmes, D. G., and Covert, E. E., "Flow-Induced Pressure Oscillations in Shallow Cavities," J. Sound Vib., Vol. 18, No. 4, 1971, pp. 545–553.

[13]Ziada, S., "Feedback Control of Globally Unstable Flows: Impinging Shear Flows," J. Fluids and Structures, Vol. 9, 1995, pp. 907–923.

[14]Roussopoulos, K., "Feedback Control of Vortex Shedding at Low Reynolds Numbers," J. Fluid Mech., Vol. 248, 1993, pp. 267–296.

[15]Ljung, L., System Identification, Prentice-Hall, Upper Saddle River, NJ, 1999.

[16]Shynk, J. J., "Adaptive IIR Filtering," IEEE ASSP Magazine, Vol. 6, No. 2, 1989, pp. 4–21.

[17]Haykin, S., Adaptive Filter Theory, Prentice-Hall, Upper Saddle River, NJ, 1996.